

Interfacial analysis and properties of regioregular poly(3-hexyl thiophene) spin-coated on an indium tin oxide-coated glass substrate

Gerald F. Malgas · Christopher J. Arendse ·
Sipho Mavundla · Franscius R. Cummings

Received: 25 February 2008 / Accepted: 9 June 2008 / Published online: 15 July 2008
© Springer Science+Business Media, LLC 2008

Abstract Interfacial analysis of the rrP3HT samples spin-coated on a glass substrate was studied in detail using transmission electron microscopy (TEM) and SEM measurements. Very homogeneous and smooth polymer (P3HT and PEDOT:PSS) layers are observed on the glass substrate. The ITO surface shows a surface roughness, with a layer of about 15 nm. Structural characteristics of the polymer blends were studied using Raman spectroscopy and photoluminescence (PL). The complete reduction of PL of P3HT after mixing with C₆₀ in a 1:1 wt.% indicates an effective charge transfer from P3HT to C₆₀. Thermo-gravimetric analysis showed that the commercially bought materials are of high purity.

Introduction

Over the last decade, the use of polymeric materials in the design and fabrication of low cost organic electronic devices,

photovoltaic devices, or plastic electronics has received much attention. Photovoltaic technology has become increasingly important as an environmentally sustainable path to world socioeconomic development. When comparing the organic technology to the silicon-based photovoltaics (PV), the two very different technologies are complementary in many ways. Organic photovoltaics (OPVs) offer low cost, low thermal budget, solution processing, flexible substrates, and a very high speed of processing [1]. A major disadvantage of organic solar cells is the low overall power conversion efficiency compared with established inorganic solar cell techniques. For a major breakthrough to take place, a significant improvement in the device efficiency-to-cost ratio is essential. There are several factors that influence the efficiency of OPVs, e.g., the structure of the polymer, the morphology of the film, the interfaces [2] between the layers (organic/metal, organic/organic), and the choice of electron acceptor and the ratio between this and the polymer [3].

Intensive research in OPVs has led to a wide variety of different structure designs and different types of hole and electron acceptor materials [4–6]. Electron donor materials efficiently used are phthalocyanines, polythiophenes, and poly(phenylenevinylenes). Representative electron acceptors are perylenes, nanorods, fullerenes, and nanotubes [7–10]. In this study, the cross-sectional SEM and TEM analyses of poly(3-hexylthiophene) (P3HT) spin-coated on an ITO/Glass substrate and the optical properties will be determined.

G. F. Malgas (✉) · C. J. Arendse · S. Mavundla ·
F. R. Cummings
National Centre for Nanostructured Materials, Council for
Scientific and Industrial Research, P.O. Box 395, Pretoria 0001,
South Africa
e-mail: GMalgas@csir.co.za

S. Mavundla
Department of Chemistry, University of the Western Cape,
Private Bag X17, Bellville 7535, South Africa

F. R. Cummings
Department of Physics, University of the Western Cape,
Private Bag X17, Bellville 7535, South Africa

F. R. Cummings
Energy and Processes, Council for Scientific and Industrial
Research, Materials Science and Manufacturing, P.O. Box 395,
Pretoria 0001, South Africa

Experimental details

Sample preparation

The solar cell structures were prepared according to the following procedure. All chemicals were purchased from

Sigma Aldrich. The ITO coated on 1 mm glass substrates, with a resistance $\leq 20 \Omega/\text{square}$, was first cleaned thoroughly with solvents and dried in dry nitrogen. A thin layer of poly (3,4-ethylenedioxythiophene):poly (styrenesulfonate) (PEDOT:PSS) solution was spin-coated onto the ITO structure. The spinning rate and time of spin-coating were between 2000 and 3000 rpm and 30 s. The PEDOT layer was subsequently annealed in ambient at 100 °C for 15 min on a hotplate. The active layer containing regioregular poly (3-hexylthiophene) (rrP3HT) was dissolved in 1 mL of chloroform solution and spin-coated on top of the PEDOT:PSS layer (Sample A). For the blended sample B, rrP3HT (~ 5 mg) and C_{60} (~ 5 mg) were dissolved in 1 mL of chloroform solution. The solution was stirred overnight on a hotplate at 50 °C. The precursor solution prepared for this study had a molar concentration of 0.15 M. The solution was spin-coated on top of the PEDOT:PSS layer. The spinning rate and time of spin-coating were 2500 rpm and 30 s. In this study, no Al top electrode depositions were done on the P3HT/PEDOT:PSS/ITO/Glass structures.

Characterization

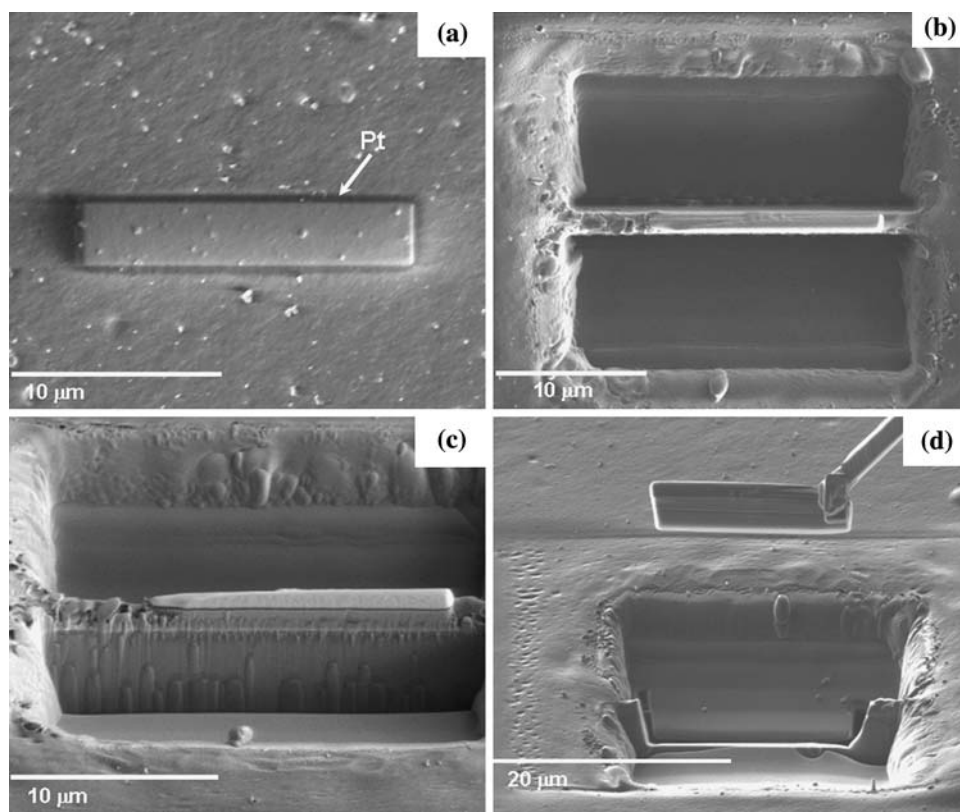
A HELIOS NanoLab 600 SEM equipped with an Elstar electron column for high resolution and contrast, as well as a Sidewinder ion column for fast, precise cross sectioning, was employed for cross-sectional and interfacial analysis of the

material spin-coated on the glass substrate. All chemicals were used as received without further purification; however, thermo-gravimetric analysis (TGA) (stability measurements) was performed using a Perkin-Elmer thermo gravimetric analyzer. Measurements were carried out in an O_2 atmosphere at a heating rate of 10 °C/min from room temperature to 950 °C. The photoluminescence (PL) spectra were measured by exciting the samples with 350 nm line of deuterium lamp. The emission was detected with Jobin Yvon PMT detector. The Raman measurements were performed using a Horiba Jobin Yvon HR800 micro-Raman spectrometer. In all measurements, an excitation wavelength of 514 nm was directed perpendicular to the substrate and the spectral resolution was set to 0.33 cm^{-1} . It should be noted that for some Raman spectroscopy and PL measurements, the PEDOT:PSS layer was omitted to avoid masking of P3HT features which overlap with those of PEDOT.

Results and discussion

Cross-sectional high resolution SEM was performed by means of ion-beam milling in the HELIOS Nanolab 600 on the polymer samples spin-coated onto the glass substrates. Descriptions of how the focused ion beam (FIB) is used to prepare cross sections and TEM specimens can be found elsewhere [11–16]. Figure 1 shows the scanning electron

Fig. 1 SEM images showing the lamella preparation of the specimen for cross-sectional viewing



micrographs of (a) the area of interest with a Pt layer deposited onto the sample to protect it during subsequent ion milling, (b) the two large trenches that are milled on either side of the area of interest in sample, (c) the area of interest at a tilted angle, and the final releasing cut that was performed, Fig. 1d, respectively. The micrograph in Fig. 1d clearly shows that the lamella is removed from the bulk of the sample for SEM and TEM analyses. When the sample is milled, a part of the material is re-deposited at nearby sample locations, especially at the sidewalls of the milled trench. The cross section surface itself usually remains clean due to the permanent milling, as shown in Fig. 2c.

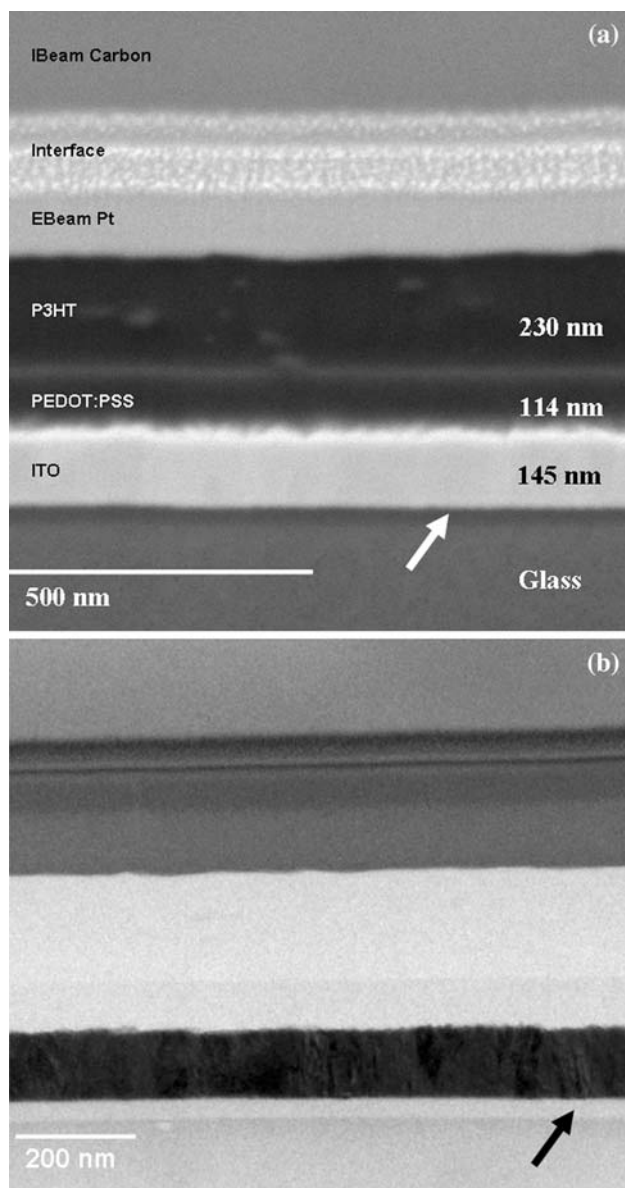


Fig. 2 High-resolution (a) SEM and (b) TEM image of a cross sectional sample of an organic layer spin coated onto an ITO coated glass substrate (sample A)

Figure 2 shows the SEM and TEM micrographs of the cross section of a Glass/ITO/PEDOT:PSS/P3HT sample (sample A). The glass, ITO, PEDOT:PSS, and P3HT in the stack are clearly visible and allow characterization of the interface. It is interesting to see that the two polymer layers exhibit different contrast and thus can be easily identified, allowing interface quality characterization of the layers. The ITO layer displays a high surface roughness of about 15 nm. According to the cross-sectional analysis, a thin interfacial layer between the glass substrate and the ITO was observed in both the SEM and TEM micrographs as shown by the arrow indicators. This layer might have been introduced during the ITO/Glass sample preparation. Hong et al. [17] showed that an ITO film deposited on a barrier layer improves the optical and electrical properties of the ITO film. They showed that using TiO_2 as a barrier layer improves the resistance to moist heat and surface uniformity more effectively than using SiO_2 as a barrier layer.

It can also be seen that the PEDOT/PSS layer forms a very smooth interface with the organic layer (P3HT), thus reducing the stress on the active layer during operation, which otherwise results from high local electric fields at peaks on the ITO surface. Peumans et al. [18] reported that spin-coating the ITO anode with a PEDOT:PSS layer improved the photovoltaic cell efficiency. They showed that the fill factor (FF) can be significantly improved by treating the PEDOT:PSS surface with a mild Ar or O_2 plasma, further suggesting the importance of this interface. It is also evident that small pores with different diameters are present in the P3HT polymer layer. The results show that the active P3HT layer has a thickness of ~ 230 nm. Gebeyehu et al. [19] reported that the thickness of semi-conducting organic films represents a crucial parameter for their performance in photovoltaic devices. They also showed that the need to absorb most of the sunlight in solar cells requires a film thicker than 100 nm. On the other hand, thin layers enhance the internal electric field and improve the charge transport.

To estimate the thermal stability of P3HT and fullerene, TGA analysis was performed in an O_2 atmosphere. Figure 3 shows the TGA and the differential thermal analysis (DTA) of (a) P3HT and (b) fullerene as measured in O_2 . In a typical experiment, nearly equal amounts (~ 4 mg) of P3HT and fullerene were loaded into a platinum pan for TGA under constant oxygen flow. The temperature upper limit was set at 900 $^\circ\text{C}$ with a relatively slow scanning rate of 10 $^\circ\text{C}/\text{min}$ to ensure complete thermalization of the polymer and fullerene.

It is clear from Fig. 3a that the polymer is very stable against thermal decomposition. It is observed that the mass loss takes place in a two-step mechanism. The DTA consists of two maxima at temperatures around 465 and 635 $^\circ\text{C}$ as shown in Fig. 3a indicating two different

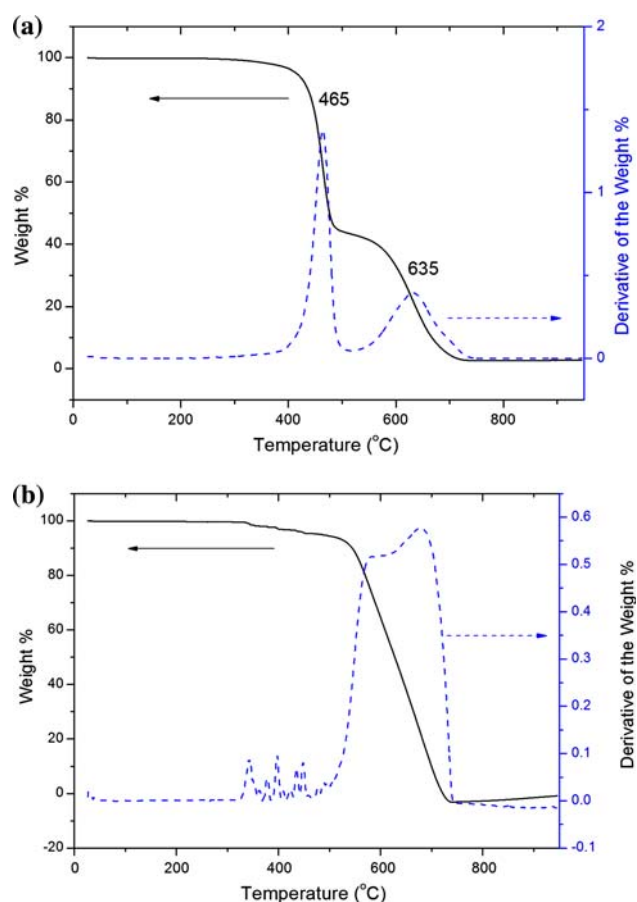


Fig. 3 TGA profile of (a) P3HT and its first derivative plot, showing two stages of decompositions at 465 and 635 °C and (b) fullerene (C60) and its first derivative

components of similar oxidation behavior. The first step of the mass loss began at about 460 °C and the second step began at about 600 °C. Such an oxidation at high temperature obviously cannot be due to physisorbed species. The beginning of the mass loss might be due to the loss of an alkyl side group attached to the aromatic thiophene backbone (hexyl group). As the temperature increases above 500 °C, the oxidation is accelerated and the pyrolysis of the aromatic backbone of polymer chains is ignited. The thermal analysis graphs of the fullerene in Fig. 3b shows that the initial degradation temperature (IDT) takes place at 530 °C while the mass loss occurs between 550 and 730 °C. The thermo-gravimetric analysis under oxygen between room temperature and 950 °C showed a zero percentage remaining mass indicating that the purchased materials are of highly pure quality.

Figure 4 shows the Raman spectroscopy of the P3HT films as well as different blends of P3HT:C₆₀ films deposited on a Si substrate. The samples were excited by a 514 nm laser in the frequency range of 200–2000 cm⁻¹. The spectrum of the poly(3-hexylthiophene) film deposited

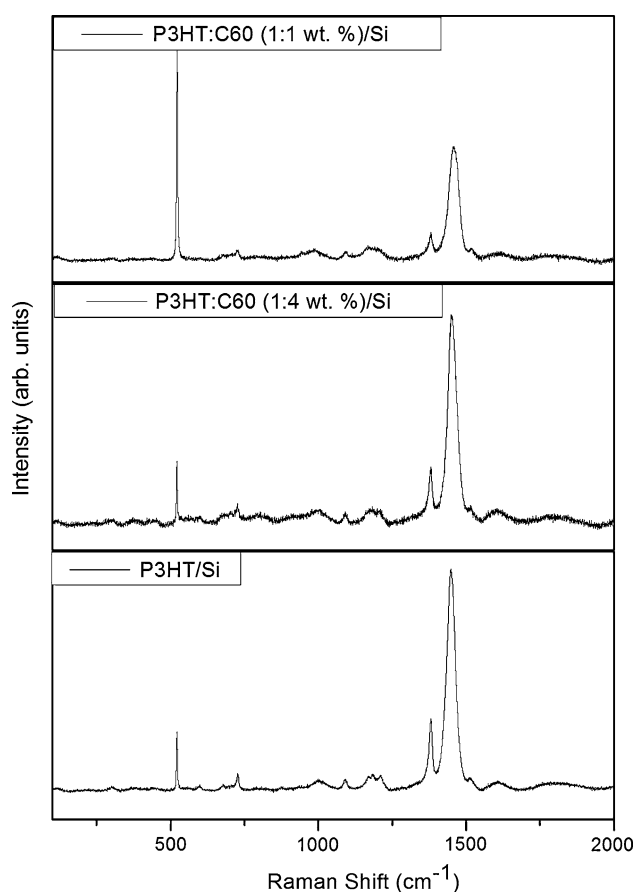


Fig. 4 Raman spectra of (a) P3HT, (b) P3HT:C₆₀ (1:4 wt.%) and (c) P3HT:C₆₀ (1:1 wt.%), films spun on a Si substrate

on Si is identical to previous results for regioregular P3HT (rrP3HT); it features all vibrational frequencies expected for the conjugated polymer [20]. The signals in the range 1445–1460 cm⁻¹ correspond to the symmetric C_α=C_β stretching deformation, while the medium intensity band at 1375–1380 cm⁻¹ is associated with C_β-C_β stretching deformations in the aromatic thiophene ring [21, 22]. No Raman features attributable to C₆₀, such as the A_{1g}1469 cm⁻¹ mode of fullerenes could be resolved. Klimov et al. [23] showed that the contributions of the C₆₀ fluorescence are not expected to influence the Raman modes of P3HT in the blends. To extract additional information from the Raman spectra (e.g., peak positions, relative intensities, and full width at half-maximum (FWHM)), curve fittings were carried out with a Lorentzian function and summarized in Table 1.

It can be seen from Table 1 that the peak position, corresponding to the symmetric C_α=C_β stretching deformation, is shifted to a higher wavenumber (cm⁻¹), if the polymer is blended with C₆₀. A downward shift in the wavenumber generally indicates an increase in the crystallinity of P3HT polymer and the extension of the effective conjugation length along the polymer backbone

Table 1 Raman measurement for the P3HT/Si films as well as different blends of P3HT:C60

Sample	C_{β} - C_{β} stretching deformations				C_{α} - C_{β} stretching deformations			
	Area	Peak position (cm^{-1})	FWHM	Intensity	Area	Peak position (cm^{-1})	FWHM	Intensity
P3HT/Si	94443	1380.3	12.115	4963.0	1.1782E6	1449.3	36.889	20333
P3HT:C ₆₀ (1:1 wt.%/Si)	15478	1379.4	13.101	752.12	4.0067E5	1458.1	45.877	5559.9
P3HT:C ₆₀ (1:4 wt.%/Si)	31434	1379.8	12.498	1601.1	5.3726E5	1453.2	39.453	8669.3

[24]. As a result, the polymer film prepared with a C₆₀-fullerene has the favorable molecular morphologies for the transport of charge carriers and is also responsible in the improvement of cell efficiencies. Interesting effects on the FWHM of the peak can be observed. The FWHM increases with the addition of C₆₀-fullerene as shown in Table 1. This change in the FWHM is consistent with the changes observed in the PL intensity.

Sariciftci et al. [25] showed that the comparison of the PL of a donor with that of the donor/acceptor composite provides an important, but also simple, method to detect the charge transfer (CT), which is indicated by the quenching effect of the composite. Figure 5 compares the PL spectra of P3HT film with that of blends of P3HT with different fullerene ratios. The P3HT shows PL, which is completely quenched when it is mixed with a 1:1 wt.% of C₆₀. This implies that the excitons generated on one polymer within the film reached an interface with the other polymer and dissociate before recombining. As shown in Fig. 5, the PL spectra of the blend of P3HT:C₆₀ 1:4 wt.% show a blue shift (downwards shift) compared to the spectra of a neat film of P3HT, suggesting that the polymer chains are twisted and not π -stacked on each other. At this point, it is unclear whether the incomplete quenching resulted from reduced exciton mobility on the polymer chains or from the pore size simply being too large given the small exciton diffusion length that has been observed in

thiophene-based polymers [26]. Al-Ibrahim et al. [27] reported that materials with high absorption coefficient are necessary for application in polymer solar cells, because the film thickness of the photoactive layer should not be normally over some hundreds of nanometers (typical are 100–300 nm). This limitation is predicted by the much lower charge mobility compared with inorganic semiconductors.

Conclusion

SEM and TEM analyses of the cross sections revealed that a smooth and homogeneous polymer (P3HT and PEDOT:PSS) film is observed on the glass substrate. The ITO/Glass substrate has an interfacial surface roughness of ~ 15 nm, while the most sensitive organic layers have sharp and undistorted interfaces. Thermal stability of the polymer (P3HT) and fullerene showed that the commercially bought materials are of high purity. The results show that the polymer is very stable against thermal decomposition until around 400 °C and that the oxidation is completed at 730 °C. Analysis of the fullerene sample showed that a zero percentage mass loss was observed. The complete reduction of PL of P3HT after mixing with C₆₀ in a 1:1 wt.% indicates an effective charge transfer from P3HT to C₆₀.

Acknowledgements The authors would like to acknowledge the financial support of the Council for Scientific and Industrial Research (CSIR), South Africa (Project No: HGERA7S). The authors are very grateful to Drs. Christoph Mitterbauer and David Wall of the FEI Company (The Netherlands, Eindhoven) for helping with the microscopy analysis.

References

1. Brabec CJ, Sariciftci NS, Hummelen JC (2001) *Adv Funct Mater* 1:15. doi:10.1002/1616-3028(200102)11:1<15::AID-ADFM15>3.0.CO;2-A
2. Ishii H, Sugiyama K, Ito E, Seki K (1999) *Adv Mat* 11:605. doi:10.1002/(SICI)1521-4095(199906)11:8<605::AID-ADMA605>3.0.CO;2-Q
3. Hoppe H, Sariciftci NS (2006) *J Mater Chem* 16:45. doi:10.1039/b510618b
4. Tang CW (1986) *Appl Phys Lett* 48:183. doi:10.1063/1.96937

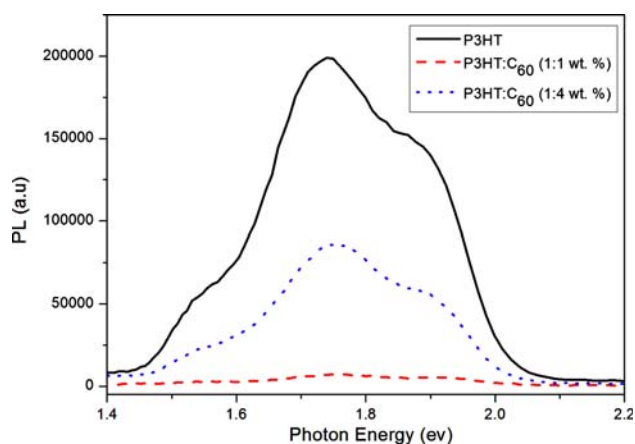


Fig. 5 Photoluminescence spectra of films of P3HT, P3HT:C₆₀ (1:1 wt.%) and P3HT:C₆₀ (1:4 wt.%) deposited on a Si substrate

5. Yu G, Gao J, Hummelen J, Wudl F, Heeger AJ (1995) *Science* 270:1789. doi:[10.1126/science.270.5243.1789](https://doi.org/10.1126/science.270.5243.1789)
6. Shaheen SE, Brabec CJ, Padinger F, Fromherz T, Hummelen JC, Sariciftci NS (2001) *Appl Phys Lett* 78:841. doi:[10.1063/1.1345834](https://doi.org/10.1063/1.1345834)
7. Halls JJM, Pichler K, Friend RH, Moratti SC, Holmes AB (1996) *Appl Phys Lett* 68:3120. doi:[10.1063/1.115797](https://doi.org/10.1063/1.115797)
8. Huynh WU, Dittmer JJ, Alivisatos AP (2002) *Science* 295:2425. doi:[10.1126/science.1069156](https://doi.org/10.1126/science.1069156)
9. Wienk MM, Kroon JM, Verhees WJH, Knol J, Hummelen JC, van Hal PA, Janssen RAJ (2003) *Angew Chem Int Ed* 42:3371. doi:[10.1002/anie.200351647](https://doi.org/10.1002/anie.200351647)
10. Kymakis E, Amaratunga GAJ (2002) *Appl Phys Lett* 80:112. doi:[10.1063/1.1428416](https://doi.org/10.1063/1.1428416)
11. Orloff J, Utlaut M, Swanson L (2003) *High resolution focused ion beams: FIB and its applications*. Kluwer Academic/Plenum Publishers, New York
12. Rowlands N, Munroe PR (1998) *Microstr Sci* 26:233
13. Phaneuf MW, Li J, Malis T (1998) *Microsc Microanal* 4 (Suppl. 2, Proceeding):492
14. Overwijk MHF, Van den Heuvel FC, Sulle-Lieuwma CWT (1993) *J Vac Sci Technol B* 11:2021. doi:[10.1116/1.586537](https://doi.org/10.1116/1.586537)
15. Giannuzzi LA, Stevie FA (1999) *Micron* 30:197. doi:[10.1016/S0968-4328\(99\)00005-0](https://doi.org/10.1016/S0968-4328(99)00005-0)
16. Cairney JM, Smith RD, Munroe PR (2000) *Microsc Microanal* 6:452
17. Hong JS, Rhee BR, Kim HM, Je KC, Kang YJ, Ahn JS (2004) *Thin Solid Films* 467:158. doi:[10.1016/j.tsf.2004.03.014](https://doi.org/10.1016/j.tsf.2004.03.014)
18. Peumans P, Forrest SR (2001) *Appl Phys Lett* 79:126. doi:[10.1063/1.1384001](https://doi.org/10.1063/1.1384001)
19. Gebeyehu D, Padinger F, Brabec CJ, Fromherz T, Hummelen JC, Sariciftci NS (1999) *Intl J Photoenergy* 1:89. doi:[10.1155/S1110662X99000185](https://doi.org/10.1155/S1110662X99000185)
20. Osterbacka R, An CP, Jiang XM, Vardeny ZV (2001) *Synthetic Metal* 116:317. doi:[10.1016/S0379-6779\(00\)00429-X](https://doi.org/10.1016/S0379-6779(00)00429-X)
21. Brown PJ, Thomas DS, Köhler A, Wilson JS, Kim JS, Ramsdale CM, Sirringhaus H, Friend RH (2003) *Phys Rev B* 67:064203. doi:[10.1103/PhysRevB.67.064203](https://doi.org/10.1103/PhysRevB.67.064203)
22. Louarn G, Trznadel M, Buisson JP, Laska J, Pron A, Lapkowski M, Lefrant SJ (1996) *Phys Chem* 100:12532. doi:[10.1021/jp960104p](https://doi.org/10.1021/jp960104p)
23. Klimov E, Li W, Yang X, Hoffmann GG, Loos J (2006) *Macromolecules* 39:4493. doi:[10.1021/ma052590x](https://doi.org/10.1021/ma052590x)
24. Heller C, Leising G, Godon G, Lefrant S, Fischer W, Stelzer F (1995) *Phys Rev B* 51:8107. doi:[10.1103/PhysRevB.51.8107](https://doi.org/10.1103/PhysRevB.51.8107)
25. Sariciftci NS, Smilowitz L, Heeger AI, Wudl F (1992) *Science* 258:1474. doi:[10.1126/science.258.5087.1474](https://doi.org/10.1126/science.258.5087.1474)
26. Theander M, Yartsev A, Zigmantas D, Sundstrom V, Mammo W, Anderson MR, Inganasm O (2000) *Phys Rev B* 61:12957. doi:[10.1103/PhysRevB.61.12957](https://doi.org/10.1103/PhysRevB.61.12957)
27. Al-Ibrahim M, Roth H, Zhokhavets U, Gobsch G, Sensfuss S (2005) *Solar Energy Mater Solar Cell* 85:13